

Characterizing the effect of substrate surface roughness on particle-wall interaction with the airflow method

Yanbin Jiang¹, Shuji Matsusaka^{2*}, Hiroaki Masuda² and Yu Qian¹

1. School of Chemical and Energy Engineering, South China University of Technology, Guangzhou 510640, China
2. Department of Chemical Engineering, Kyoto University, Kyoto 615-8510, Japan

Abstract

The effect of surface roughness on particle-wall interaction was studied by the airflow method. Five kinds of monodispersed spherical particles ($D_{p50} = 11\text{--}41\ \mu\text{m}$) and six test pieces with different surface roughness ($Ra = 0.01\text{--}1.64\ \mu\text{m}$) were used in the experiments. The particles were dispersed on the test pieces to form a monolayer, and entrained in a rectangular air channel. The air velocity increased at a constant rate, and the entrained particles were detected with a laser dust monitor. Microscopic observations showed that particle entrainment occurred in discrete and intermittent events during experiment, thus a statistical parameter, i.e. the particle entrainment efficiency as a function of the air velocity, was defined for evaluating the particle-wall interaction force distribution. The experimental results showed that the air velocity for particle entrainment decreases with the increase of the surface roughness within submicron-scale and reaches a lower limit, while increases to some extent for micron-scale surface roughness. It was also found that the effect of the substrate surface roughness depends on the particle diameter.

Keywords: particle-wall interaction; adhesion; surface roughness; airflow method; entrainment

* Corresponding author. *E-mail address:* matsu@cheme.kyoto-u.ac.jp (S. Matsusaka)

1. Introduction

The interaction force between a particle and a solid surface plays an important role in powder handling processes, such as pneumatic transport, dry dispersion, classification and many others. Although the mechanisms governing the interaction force have been extensively studied in the past, they are not well understood. In fact, there are many factors affecting the interaction force, e.g. particle size, shape, roughness, material properties, and environmental conditions. Among of them, surface roughness is very important for powder handling processes [1-3], since the interaction force can be effectively changed with the wall surface without changing the particle properties. Up to now, it is difficult to theoretically predict the actual interaction forces and their distributions accurately, thus experimental approach is required for the evaluation.

Over the past few decades, many techniques have been developed to characterize the particle-wall interactions, e.g. atomic force microscopy (AFM) [4-7], centrifugal methods [8, 9], airflow methods [9-12]. AFM can analyze the interaction forces in detail, but the sample preparation is not easy and usually carried out for a single particle measurement, thus it is not suitable for statistical measurement of many particles. The centrifugal methods can obtain interaction force distributions by systematically changing the centrifugal force [8], it is, however, not easy to measure automatically because of the difficulty in incorporation of a detecting system into the centrifuge. It is time-consuming if the operation has to be manually performed. On the other hand, the airflow method can measure the interaction force distributions in a short time by a simple operation.

In this paper, particle-wall interaction is studied using the airflow method, particularly focusing on the effect of the substrate surface roughness and particle diameter.

2. Experimental

2.1. Apparatus and procedure

Fig. 1 shows a schematic diagram of the experimental apparatus for characterizing particle-wall interaction. The principle of the airflow method has been discussed elsewhere [9-12]. For the preparation of the experiment, particles were deposited on the flat surface of

a test piece, 40 mm long and 10 mm wide, made of stainless steel (JIS SUS 316). To disperse the particles uniformly on the surface, a sieve with mesh size of 45 μm was used. Additionally, a mask sheet was used to deposit the particles at the center area of $25 \times 4 \text{ mm}^2$ along the lengthways direction of the test piece. A small number of agglomerated particles on the surface were easily removed by tapping under gravity. With this procedure, the micro-particles were deposited as a monolayer on the test piece.

Feiler et al pointed out that particle adhesion is rather low at lower humidities, but it increases significantly above a threshold value which is around 55% relative humidity [13]. A similar result can be found in the paper by Paaanen et al [14]. It is also pointed out that the adhesion varies according to the exposure time, even though it is longer than 1h at high humidity (above 60% RH) [13]. Thus, to avoid the effect of humidity on the adhesion, the particle deposition was completed in a short time of five minutes at 35-50 % RH and 17-20 $^{\circ}\text{C}$. The test piece was mounted flush with the inside surface of a rectangular air channel, 1.0 mm high, 8.0 mm wide, and 140 mm long, and the entrainment experiment was carried out. The top of the channel was made of glass for observing the entrainment of particles by a high-speed microscope camera (Fastcam-Max, Photron Ltd.).

Clean compressed air was dried to a relative humidity of 10% and supplied in the channel, the air velocity in the channel was controlled with a computer so as to increase at a constant rate ($\alpha = 0.5 \text{ m/s}^2$). When the aerodynamic drag force exceeds the particle-wall interaction, the particle is entrained into the airflow. In this experiment, the particles entrained from the surface were detected with a laser dust monitor (LD-1, Sibata Scientific Technology). The airflow rate in the laser dust monitor was kept constant by supplying a secondary clean air, although the airflow rate in the channel varied during the measurement. The air velocity in the channel and the number of entrained particles were automatically recorded into the computer. For each experiment, the required measurement time was 600 seconds, and the data sampling interval was 0.1 second. The relationship between the entrainment efficiency and the air velocity was obtained by digital processing, and the median value of the air velocity \bar{u}_{50} was determined. The measurement was repeated three times for the repeatability, and average of the entrainment efficiency curves was obtained from

these data.

2.2. Test particles

Three kinds of glass beads (JIS Z 8901 GBM 20, 30, 40) and two kinds of PMMA particles (Sekisui Plastics Co., Ltd.) were used as test particles. Fig. 2 shows the SEM images of sample particles. All the particles are spherical and the particle surfaces are sufficiently smooth; the average surface roughness Ra is less than 0.1 μm . Table 1 shows the physical properties of the particles, including particle density ρ_p , the mass median diameter D_{p50} , and the geometric standard deviation of particle diameter distribution σ_g . The mass median diameter is in the range of 11 to 41 μm , the standard deviation σ_g is in the range from 1.04 to 1.11, indicating narrow size distributions of particle samples.

2.3. Preparation of test pieces with different surface roughness

Stainless steel test pieces (JIS SUS 316), 40 mm long and 10 mm wide, with six different levels of surface roughness on the top (S1-S6) were prepared for the experiment. The upper surface of all the test pieces were first polished to be 10 nm by wet grinding with abrasive, then mechanically abraded in the widthways direction of the test pieces using emery papers with different grains. The surface roughness was observed by a laser type confocal displacement meter (LT-8010, Keyence Corp.). Fig. 3 shows a three dimensional image of a sample test piece. The air flows perpendicularly to the direction of the roughness. Fig. 4 shows the average surface roughness Ra measured by a laser microscope (VK-8510, Keyence Corp.). Ra values were in a range from 0.01 to 1.64 μm . Fig. 5 shows the profiles of the surface roughness along the lengthways direction of the test pieces (S1-S6). Although the roughness is not perfectly uniform, the local height variation is within a certain level, depending on the condition of the mechanical surface treatment.

3. Results and discussion

3.1. Observation of particle deposition

Particles deposited on the test pieces were observed through a scanning electron microscope (VE9800, Keyence Corp.). Fig. 6 shows SEM images of the particles deposited on the test pieces with different surface roughness. It is obvious that the contact geometries of particle-wall depend on the surface roughness. For $Ra = 0.01 \mu\text{m}$, the wall surface is very

smooth compared to particle diameter. For $Ra = 0.26 \mu\text{m}$, the surface is somewhat rough. As for $Ra = 1.64 \mu\text{m}$, some particles were placed in the concavities on the rough surface of the test piece and the contact area between the particle and the surface looks larger.

3.2. Observation of particle entrainment

Rolling, sliding, and/or lifting have been proposed as possible mechanisms of the particle entrainment from a surface by airflow [9, 15-20]. Braaten et al. observed that particle entrainment occurs in discrete and intermittent events at three free-stream velocities (6.0, 7.5 and 9.0 m/s) through a laser photodiode detection system [21]. Ibrahim et al. observed the motion of individual micro-particles using a 30-fps camera with 20 times optical lens, showing that particle detachment occurred primarily as rolling motion along the surface and not as lift-off when the free-stream velocity varied from 0 to 23 m/s [22].

In our study, the airflow in the channel increased from 0 to 300 m/s with a constant rate ($\alpha = 0.5 \text{ m/s}^2$) for each experiment, and the particle entrainment from the surface was observed using a high-speed microscope camera with a frame rate of 4000 fps, an exposure time of 0.25 ms, and a magnification of 1000 times. A video with 4000 frames was recorded into a computer for each observation and carefully analyzed frame by frame. This permitted a quantitative evaluation of the progress of micro-particle entrainment in relation to flow velocity and particle diameter. The slow playback of the video showed that spherical particles were not sliding but rolling for a very short period, and immediately lifting off from the surface. This phenomenon will strongly depend on both the air velocity and the particle diameter, i.e. the period of the rolling decreased with the increase in the air velocity or the decrease in the particle diameter. Also, it was observed that particles discretely and intermittently entrained from the surface of the test piece.

Typical snapshots of the particle entrainment were shown in Fig. 7. The entrained particle, which was enclosed with a white ellipse, was carried downstream with an increasing velocity. The moving velocity during the rolling motion at initial stage ($< 1 \text{ ms}$) was very low but became high after lifting off ($> 1 \text{ ms}$). Although there are many particles on the test piece, the entrained particle did not collide with other particles. This is because the particle was carried away from the surface toward the main flow at an early stage of the entrainment.

In fact, the collisions between entrained particles and other particles were seldom observed in all experiments.

3.3. Entrainment efficiency and repeatability of the airflow method

Since the particle-wall interaction depends on the individual contact state, the air velocity for each particle entrainment is not constant. Therefore, the particle-wall interactions have to be evaluated statistically. The distribution function can be analyzed by the particle entrainment efficiency η , which is represented with the number ratio of entrained particles to total particles, i.e.

$$\eta = \int_0^{\bar{u}} n' d\bar{u} / \int_0^{\infty} n' d\bar{u} \quad (1)$$

where \bar{u} is the cross-sectional average air velocity, n' is the differential coefficient of the normalized number of entrained particles with respect to the average air velocity.

Few investigations have reported the repeatability of the results for micro-particle detachment from a substrate. Fig.8 shows the particle entrainment efficiency as a function of the average air velocity; there are three measurements obtained under the same conditions. It indicates that the repeatability is reasonably good for the airflow method, and the experimental error of the measurements is within 10%.

For applying the experimental results to other systems, the wall shear stress τ_w should be used as the evaluation factor due to its physical meaning in a turbulent boundary layer. The wall shear stress τ_w in the channel is calculated by the following equation [18].

$$\tau_w = 0.0396 \rho (\nu / D_e)^{1/4} \bar{u}^{7/4} \quad (2)$$

where ρ is the density of air, ν is the dynamic viscosity of air, and D_e is the equivalent diameter of the rectangular channel. For reference, the scale of τ_w is added on the top of the transverse axis in Fig 8a, 9a, and 10a.

3.4. Effect of surface roughness and particle diameter on entrainment

Figs. 9 and 10 show the relationships between the entrainment efficiency and the average air velocity for glass beads and PMMA particles, respectively. The entrainment efficiency depends on the average surface roughness Ra . When the surface roughness is in nano-scale

and submicron-scale, the entrainment efficiency curves tend to shift toward lower air velocities with increasing surface roughness. As for micron-scale of surface roughness, the entrainment efficiency curves shift toward the opposite direction. It is also found that the entrainment efficiency curves shift toward lower air velocities with the increase of particle diameter, and the distribution of the entrainment efficiency curves becomes narrow.

For easier understanding of the effect of surface roughness on the entrainment, we use a median entrainment air velocity \bar{u}_{50} , i.e. the air velocity at which 50% of the sample particles are entrained. Fig. 11 shows the relationship between \bar{u}_{50} and average surface roughness Ra . The value of \bar{u}_{50} decreases with the increase of surface roughness, and becomes smallest at submicron roughness (about 0.3 μm). The value tends to increase when the surface roughness is in micron-scale. This phenomenon becomes more obvious for smaller particles. Submicron-scale surface roughness increases the effective contact gap and decreases the actual contact area corresponding to the asperities in the apparent contact area. Consequently, the particle-wall interaction decreases with the increase of submicron-scale surface roughness. However, because of the geometrical effect, micron-scale surface roughness does not effectively reduce the interaction force. When particles are placed between asperities on a rough surface, the interaction force might become larger because of the increase in the contact area, as shown in Fig. 6. Fig. 12 shows the examples of the particles remaining in the concavity on rough surface of a test piece after experiment. The number of remaining particles was less than 1% for $D_{p50}=11 \mu\text{m}$. If the particle diameter is less than several micrometers, the geometrical effect will be much larger.

Lastly, the effect of particle diameter on the particle-wall interaction for glass beads is briefly discussed. Here, the above geometrical effect is excluded from the consideration, and the surface roughness Ra is limited in the range from 0.01 to 0.26 μm . Fig. 13 shows the relationship between the entrainment air velocity \bar{u}_{50} and the particle diameter D_{p50} . For $Ra = 0.01 \mu\text{m}$, the entrainment air velocity decreases with increasing particle diameter. The decreasing ratio, however, decreases with the increase of submicron-scale surface roughness ($Ra > 0.03 \mu\text{m}$, $D_{p50} > 30 \mu\text{m}$). Therefore, the effect of the surface roughness on the particle-wall interaction should be evaluated taking into account the particle diameter.

4. Conclusion

The effect of surface roughness on particle-wall interaction has been studied experimentally. Five kinds of monodispersed spherical particles ($D_{p50} = 11\text{--}41\ \mu\text{m}$) were dispersed on the test pieces and entrained in the air channel. The entrained particles were not sliding but rolling for a very short period, and immediately moving away from the surface, consequently the particles seldom collide with other particles.

The entrainment air velocity was widely distributed and thus the particle entrainment efficiency was obtained as a function of the average air velocity. The experimental error of the measurements was within 10%. The entrainment air velocity \bar{u}_{50} decreased with the increase of surface roughness within submicron-scale, and becomes smallest at $Ra \approx 0.3\ \mu\text{m}$. Micron-scale surface roughness, however, does not effectively reduce the interaction force because of the geometrical effect. This phenomenon becomes more obvious for smaller particles.

Acknowledgement

The authors gratefully acknowledge the support from Kyoto Prefecture Collaboration of Regional Entities for the Advancement of Technological Excellence, JST, and the National Scientific Fund of China (20536020, 20676046). The authors are also grateful to Sekisui Plastics Co., Ltd. for providing the sample particles

References

- [1] H. Rumpf, Die Wissenschaft des Agglomerierens, Chemie-Ingenieur-Technik, 46 (1974) 1-11.
- [2] M. Götzinger, W. Peukert, Particle adhesion force distributions on rough surfaces, Langmuir, 20 (2004) 5298-5303.
- [3] J. Katainen, M. Paajanen, E. Ahtola, V. Pore, J. Lahtinen, Adhesion as an interplay between particle size and surface roughness, J. Colloid Interface Sci., 304 (2006) 524-529.
- [4] G. Binnig, C. F. Quate, Ch. Gerber, Atomic force microscope, Phys. Rev. Lett., 56 (1986) 930-933.
- [5] P. M. Claesson, T. Ederth, V. Bergeron, M. W. Rutland, Techniques for measuring

- surface forces, *Adv. Colloid Interface Sci.*, 67 (1996) 119-183.
- [6] B. Cappella, G. Dietler, Force-distance curves by atomic force microscopy, *Surf. Sci. Rep.*, 34 (1999) 1-104.
- [7] M. Götzinger, W. Peukert, Dispersive forces of particle-surface interactions: direct AFM measurements and modelling, *Powder Technol.*, 130 (2003) 102-109.
- [8] H. Krupp, Particle adhesion, Theory and experiment, *Adv. Colloid Interface Sci.*, 1 (1967) 111-239.
- [9] S. Matsusaka, M. Koumura, H. Masuda, Analysis of adhesive force between particle and wall based on particle entrainment by airflow and centrifugal separation, *Kagaku Kogaku Ronbunshu*, 23 (1997) 561-568.
- [10] H. Masuda, S. Matsusaka, K. Imamura, A new method for measurement of powder characteristics based on reentrainment phenomena, *KONA (Powder and Particle)*, 12 (1994) 133-143.
- [11] S. Matsusaka, K. Mizumoto, M. Koumura, H. Masuda, Evaluation of adhesive strength distribution based on reentrainment phenomena –Distribution between particle-particle and particle-wall interaction, *J. Soc. Powder Technol. Japan*, 31 (1994) 719-725.
- [12] Y. Jiang, S. Matsusaka, H. Masuda, T. Yokoyama, Characterizing the effect of surface morphology on particle-wall interaction by airflow method, *Adv. Powder Technol.*, 17 (2006) 413-424.
- [13] A. A. Feiler, J. Stiernstedt, K. Theander, P. Jenkins, M. W. Rutland, Effect of capillary condensation of friction force and adhesion, *Langmuir*, 23 (2007) 517-522.
- [14] M. Paajanen, J. Katainen, O. H. Pakarinen, A. S. Foster, J. Lahtinen, Experimental humidity dependency of small particle adhesion on silica and titania, *J. Colloid Interface Sci.*, 304 (2006) 518-523.
- [15] Y. Kousaka, K. Okuyama, Y. Endo, Re-entrainment of small aggregate particles from a plane surface by air stream, *J. Chem. Eng. Japan*, 13 (1980) 143-147.
- [16] S. G. Yiantsios, A. J. Karabelas, Detachment of spherical microparticles adhering of flat surfaces by hydrodynamic forces, *J. Colloid Interface Sci.*, 176 (1995) 74-85.
- [17] D. Kaftori, G. Hetsroni, S. Banerjee, Particle behavior in the turbulent boundary layer. I. Motion, deposition, and entrainment, *Phys. Fluids*, 7 (1995) 1095-1106.
- [18] S. Matsusaka, H. Masuda, Particle reentrainment from a fine powder layer in a turbulent air flow, *Aerosol Sci. and Technol.*, 24 (1996) 69-84.
- [19] W. Theerachaisupakij, S. Matsusaka, Y. Akashi, H. Masuda, Reentrainment of deposited particles by drag and aerosol collision, *J. Aerosol Sci.*, 34 (2003), 261-274.
- [20] G. Ziskind, Particle resuspension from surfaces: Revisited and re-evaluated, *Reviews in Chemical Engineering*, 22 (2006) 1-123.

- [21] D. A. Braaten, K. T. Paw U, R. H. Shaw, Particle resuspension in a turbulent boundary layer—observed and modeled, *J. Aerosol Sci.*, 21 (1990), 613-628.
- [22] A. H. Ibrahim, P. F. Dunn, R. M. Brach, Microparticle detachment from surfaces exposed to turbulent air flow: controlled experiments and modeling, *J. Aerosol Sci.*, 34 (2003), 765-782.

Table 1. The property of test particles.

No	Material	ρ_p (kg/m ³)	D_{p50} (μ m)	σ_g (-)
1			22	1.11
2	Glass	4200	30	1.07
3			41	1.04
4	PMMA	1200	11	1.07
5			16	1.06

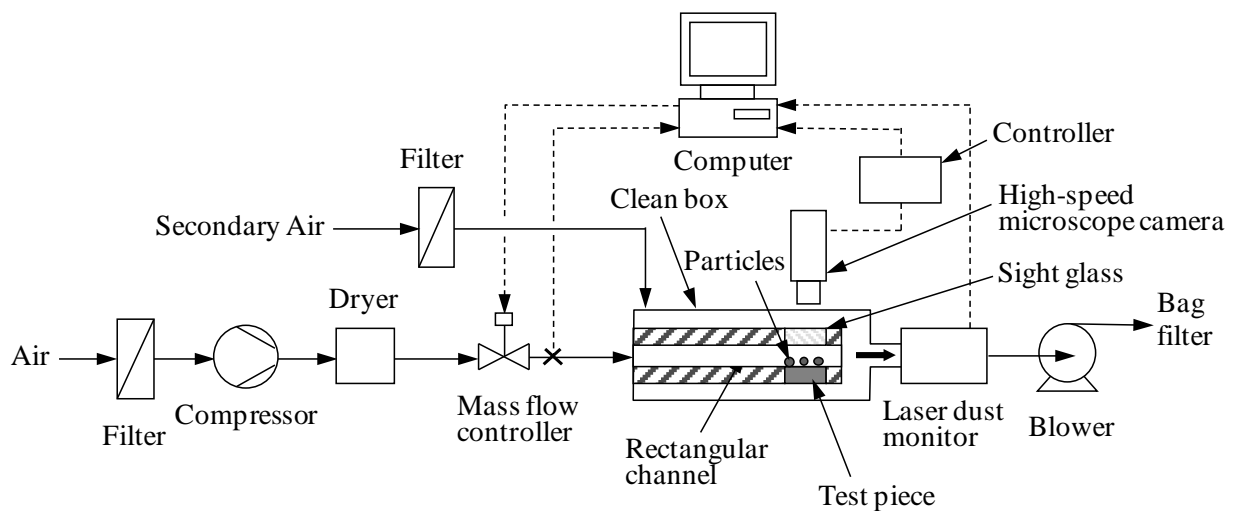
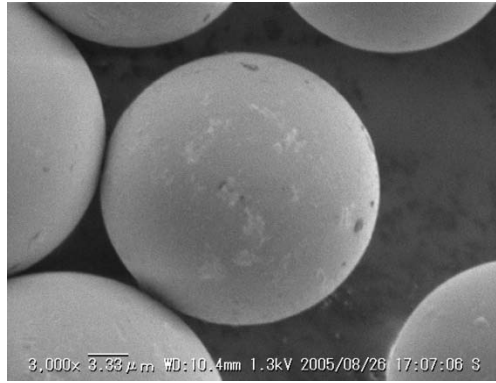
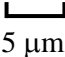
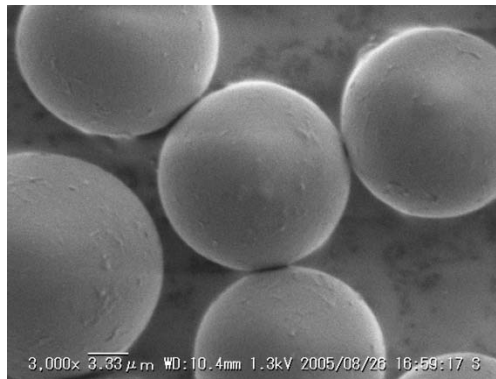


Fig. 1. Experimental apparatus for characterizing particle-wall interaction based on the airflow method.



(a) Glass beads ($D_{p50} = 22 \mu\text{m}$) 



(b) PMMA particles ($D_{p50} = 16 \mu\text{m}$)

Fig. 2. SEM images of test particles.

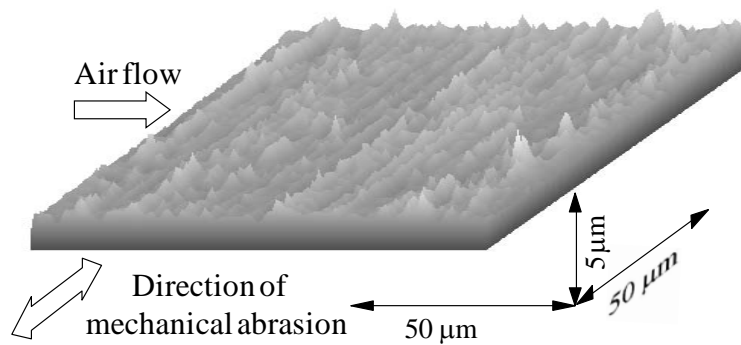


Fig. 3. Three dimensional image of surface roughness of a test piece ($Ra = 0.12 \mu\text{m}$).

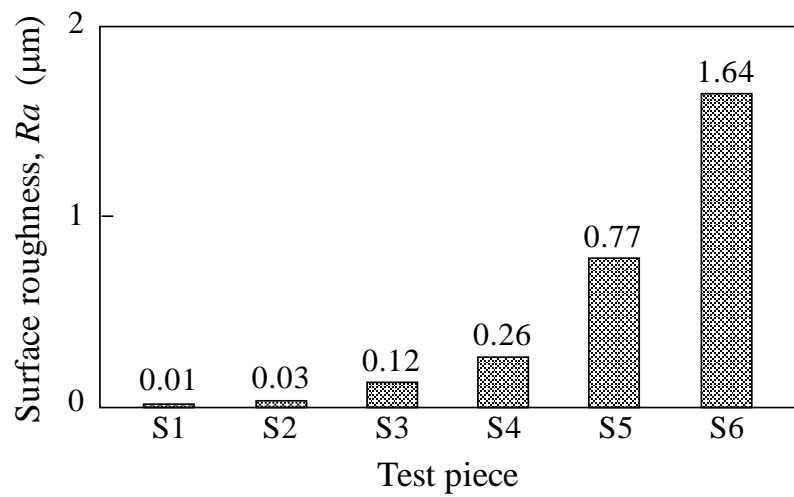


Fig. 4. Average surface roughness of the test pieces.

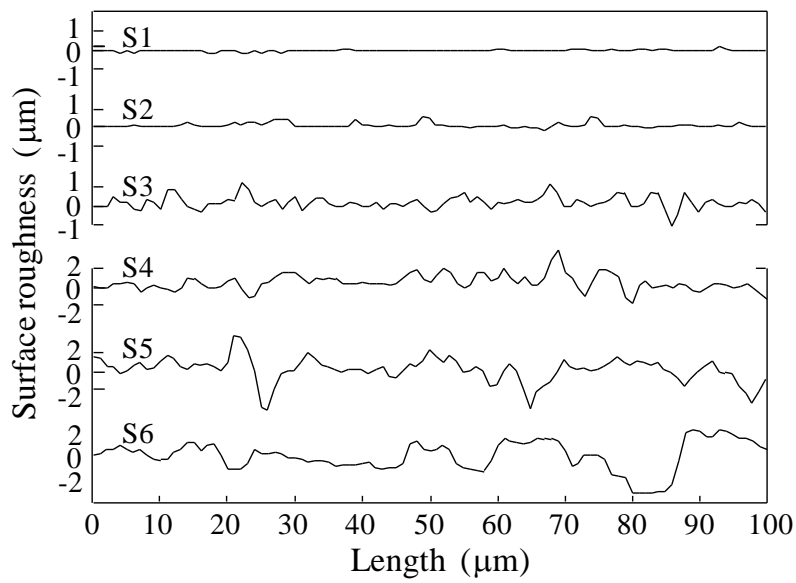


Fig. 5. Profiles of surface roughness of the test pieces.

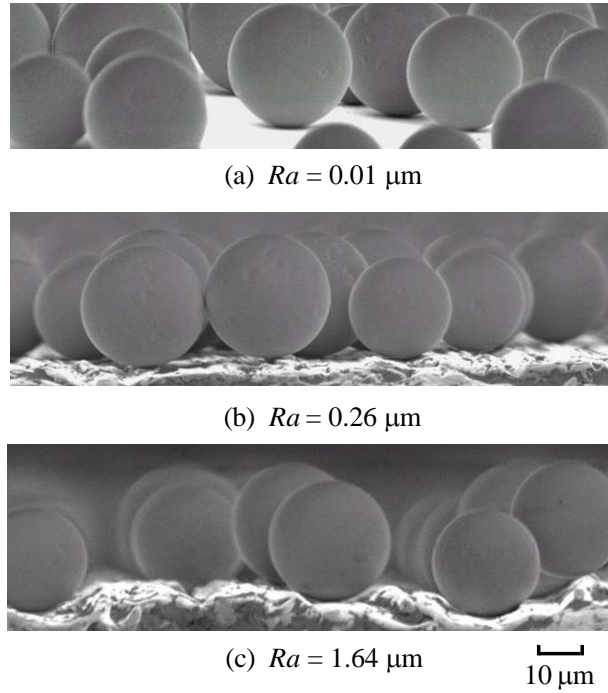


Fig. 6 SEM images of glass beads on test pieces (Glass beads, $D_{p50} = 22 \mu\text{m}$).

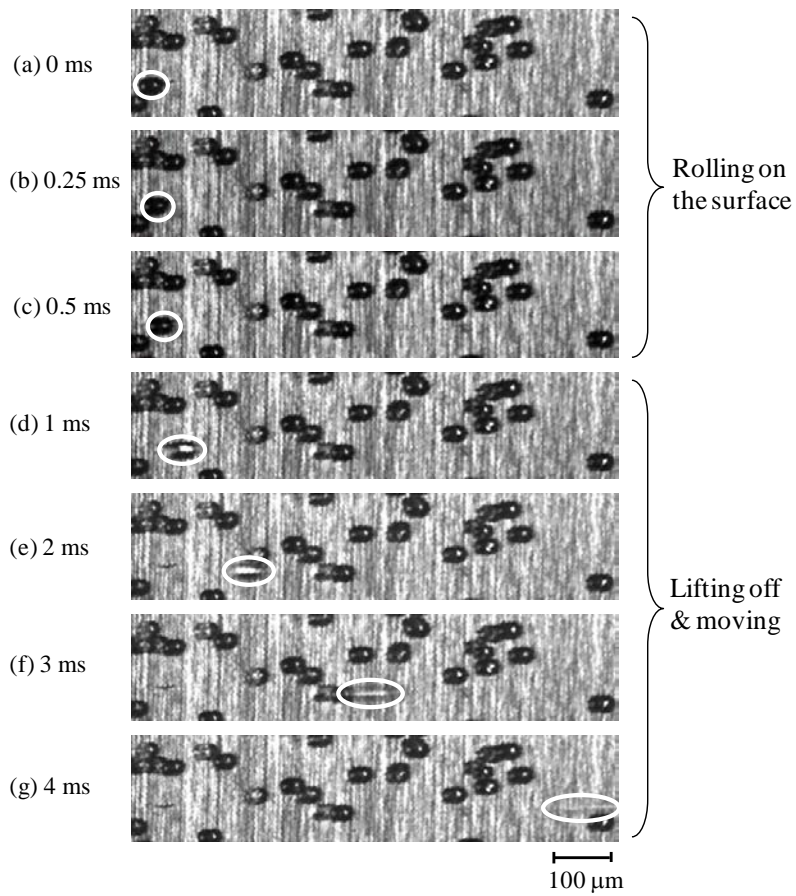


Fig. 7. Snapshots of an entrained particle; exposure time: 0.25 ms (Glass beads: $D_{p50} = 30 \mu\text{m}$, test piece: $Ra = 1.64 \mu\text{m}$, air velocity: $u = 70 \text{ m/s}$).

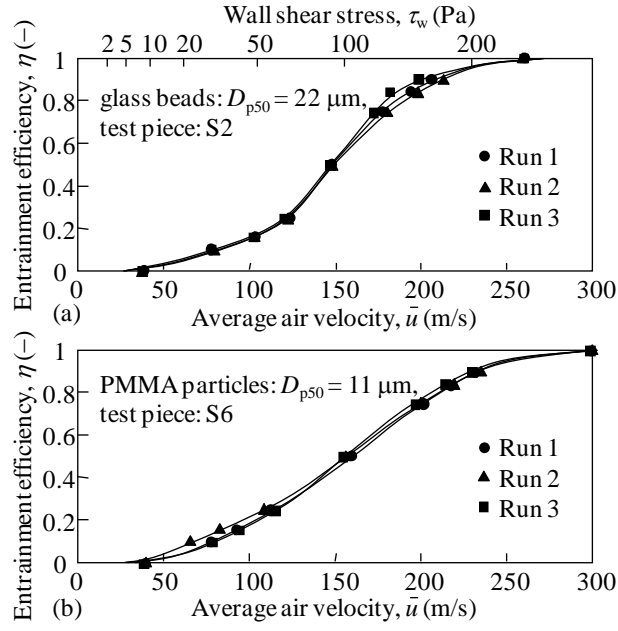


Fig. 8 Repeatability of particle entrainment efficiency.

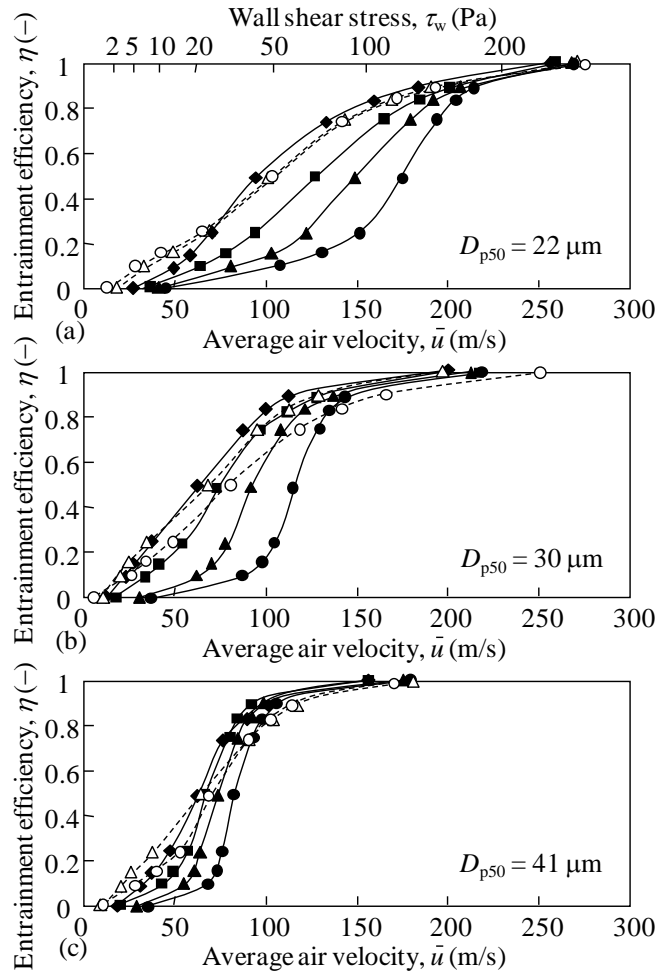


Fig. 9. Entrainment efficiency of glass beads (Ra : \bullet 0.01, \blacktriangle 0.03, \blacksquare 0.12, \blacklozenge 0.26, \triangle 0.77, \circ 1.64 μm).

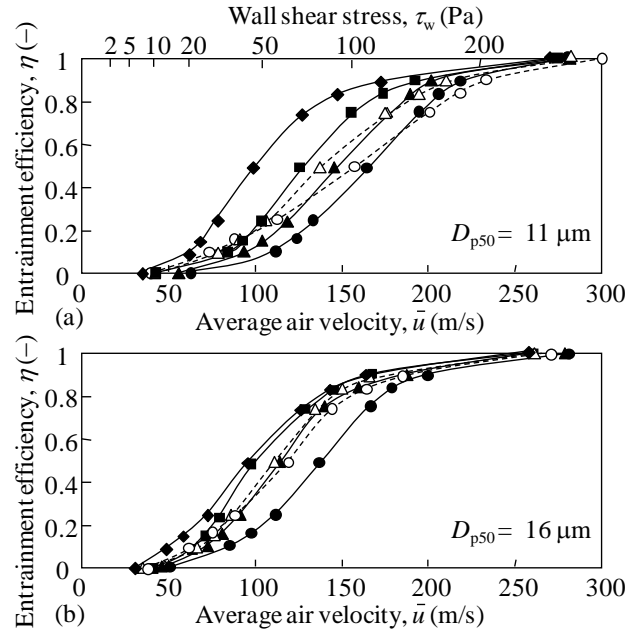


Fig. 10. Entrainment efficiency of PMMA particles (Ra : \bullet 0.01, \blacktriangle 0.03, \blacksquare 0.12, \blacklozenge 0.26, \triangle 0.77, \circ 1.64 μm).

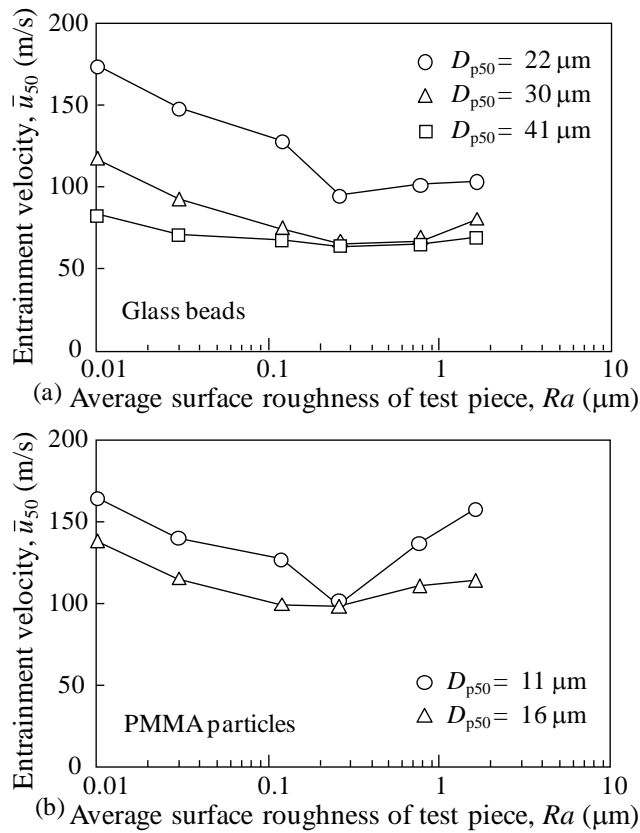


Fig. 11. Effect of the surface roughness on the entrainment velocity ((a) glass beads, (b) PMMA particles).

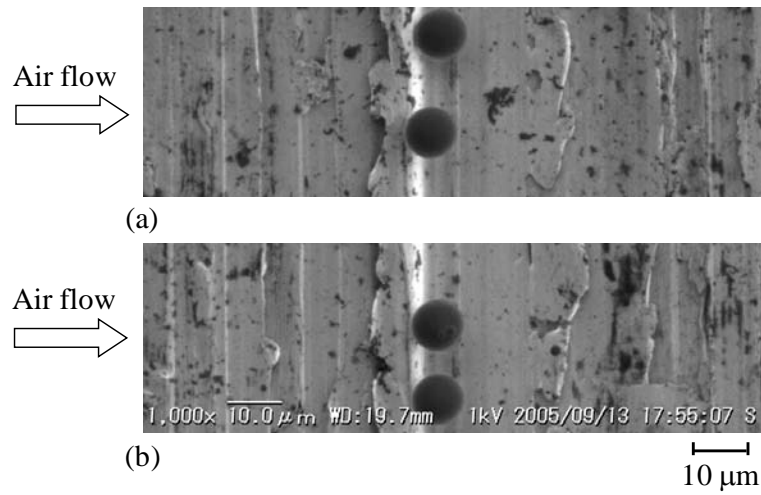


Fig. 12. SEM images of particles remaining on rough surfaces after experiment ($D_{p50} = 11 \mu\text{m}$, $Ra = 1.64 \mu\text{m}$).

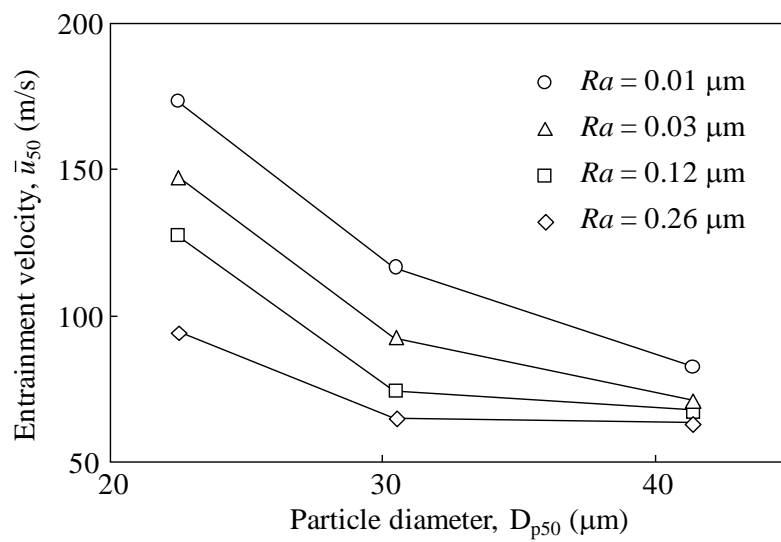


Fig. 13. Effect of particle diameter on entrainment velocity